

Article

A chromatin modulator sustains self-renewal and enables differentiation of postnatal neural stem and progenitor cells

Kushani Shah¹, Gwendalyn D. King², and Hao Jiang^{1,3,*}

¹ Department of Biochemistry and Molecular Genetics, University of Alabama at Birmingham, Birmingham, AL 35294, USA

² Department of Neurobiology, University of Alabama at Birmingham, Birmingham, AL 35294, USA

³ Department of Biochemistry and Molecular Genetics, University of Virginia, Charlottesville, VA 22908, USA

*Correspondence to: Hao Jiang, E-mail: hj8d@virginia.edu

Edited by Zhen-Ge Luo

It remains unknown whether H3K4 methylation, an epigenetic modification associated with gene activation, regulates fate determination of the postnatal neural stem and progenitor cells (NSPCs). By inactivating the Dpy30 subunit of the major H3K4 methyltransferase complexes in specific regions of mouse brain, we demonstrate a crucial role of efficient H3K4 methylation in maintaining both the self-renewal and differentiation capacity of postnatal NSPCs. Dpy30 deficiency disrupts development of hippocampus and especially the dentate gyrus and subventricular zone, the major regions for postnatal NSC activities. Dpy30 is indispensable for sustaining the self-renewal and proliferation of NSPCs in a cell-intrinsic manner and also enables the differentiation of mouse and human neural progenitor cells to neuronal and glial lineages. Dpy30 directly regulates H3K4 methylation and the induction of several genes critical in neurogenesis. These findings link a prominent epigenetic mechanism of gene expression to the fundamental properties of NSPCs and may have implications in neurodevelopmental disorders.

Keywords: neural stem cell, self-renewal, differentiation, epigenetics, H3K4 methylation, Dpy30

Introduction

The capacity of self-renewal and differentiation is the defining property of all stem cells including neural stem cells (NSCs) (Lim and Alvarez-Buylla, 2014; Bond et al., 2015). The maintenance and alteration of stem cell fate are ultimately controlled at the level of gene expression, which is profoundly shaped by the global and local chromatin state. Epigenetic mechanisms, including histone methylation, are increasingly linked to NSC fate determination (Yao et al., 2016). Histone H3K4 and H3K27 methylation marks are a paradigm of two oppositely acting epigenetic mechanisms on gene expression (Martin and Zhang, 2005; Kouzarides, 2007). Both the writer and eraser of H3K27 methylation regulate the self-renewal and/or differentiation of NSCs (Hirabayashi et al., 2009; Hwang et al., 2014; Park et al.,

2014). Bmi1, a Polycomb family protein involved in linking H3K27 methylation to gene repression, is required for NSC self-renewal partly through repressing *Ink4a/Arf* (Molofsky et al., 2003; Molofsky et al., 2005). On the other hand, the role of H3K4 methylation in NSC fate determination is relatively less understood, despite being a prominent mark generally associated with and functionally important for gene activation (Schneider et al., 2004; Jiang et al., 2013; Lauberth et al., 2013; Tang et al., 2013). Mutations of several writers, erases, and readers of this chromatin modification are associated with some human neurodevelopmental disorders (Vallianatos and Iwase, 2015), but a role of this modification in these disease processes is unknown. In mammalian cells, H3K4 methylation is mainly catalyzed by the Set1/MLL complexes, which comprise one of the Setd1a, Setd1b, Kmt2a/MLL1, Kmt2b/MLL2, Kmt2c/MLL3, and Kmt2d/MLL4 proteins as the catalytic subunit and all of the Wdr5, Rbbp5, Ash2l, and Dpy30 proteins as the common core subunits (Shilatifard, 2012). Among these subunits, MLL1 has been shown to be required for postnatal neurogenesis, but not gliogenesis (Lim et al., 2009). However, no reduction in H3K4 methylation was found either globally or at local genes in MLL1-deficient brain cells (Lim et al., 2009), suggesting that other activities of MLL1 underlie its

Received March 16, 2019. Revised March 31, 2019. Accepted April 7, 2019.
© The Author(s) (2019). Published by Oxford University Press on behalf of *Journal of Molecular Cell Biology*, IBCB, SIBS, CAS.

This is an Open Access article distributed under the terms of the Creative Commons Attribution Non-Commercial License (<http://creativecommons.org/licenses/by-nc/4.0/>), which permits non-commercial re-use, distribution, and reproduction in any medium, provided the original work is properly cited. For commercial re-use, please contact journals.permissions@oup.com

role in neurogenesis. Thus, the function of H3K4 methylation in NSC self-renewal and lineage determination remains unknown.

We have previously established a direct role of the Dpy30 subunit of the Set1/Mll complexes in facilitating genome-wide H3K4 methylation (Jiang et al., 2011) and also used an unbiased biochemical approach to show that Set1/Mll complex components are the major proteins associated with Dpy30 (Jiang et al., 2013). These results allow us to investigate the function of efficient H3K4 methylation in various biological processes by perturbing Dpy30's activity. Interestingly, Dpy30 and efficient H3K4 methylation are not essential for the self-renewal of embryonic stem cells (ESCs), but required for efficient retinoic acid-mediated differentiation of ESCs to neurons and induction of numerous neuronal lineage genes during differentiation (Jiang et al., 2011). H3K4 methylation conveys plasticity of the transcriptional program during stem cell fate transition (Jiang et al., 2011), and this is further supported by its requirement in efficient reprogramming of differentiated fibroblasts back to the pluripotent state (Yang et al., 2015). To understand a role of Dpy30 and efficient H3K4 methylation in tissue-specific stem cells, we generated a *Dpy30* conditional knockout (KO) mouse (Yang et al., 2016). Using this mouse model, we have shown a critical requirement of Dpy30 in the correct differentiation as well as long-term maintenance of hematopoietic stem cells (Yang et al., 2016). Herein, using *in vitro* and *in vivo* approaches, we sought to determine if Dpy30 and thus H3K4 methylation is involved in self-renewal and differentiation of postnatal NSCs and neural progenitor cells (NPCs, together NSPCs).

Results

Expression of Dpy30 in the developing brain

To learn the expression pattern of Dpy30 in the developing mammalian brain, we mined a collection of *in situ* hybridization images for gene expression in the developing and adult mouse nervous system (Magdaleno et al., 2006). We found that Dpy30 is mainly expressed in the hippocampus and the cerebellum starting at E15 but its expression is diminished by early adulthood (P42) (Supplementary Figure S1A). These results suggest a possible role of Dpy30 during a specific window of brain development. We next mined a single-cell RNA-sequencing (RNA-seq) data set of NSCs, NPCs, and their progeny cells in the mouse neocortex (Telley et al., 2016) and found Dpy30 is expressed at the highest level in NSCs and intermediate progenitor cells but low levels in early or late neurons (Supplementary Figure S1B). We also examined the expression of other subunits of the Set1/Mll complexes. Interestingly, all of the other core subunits, including Ash2l, Rbbp5, and Wdr5 are expressed at low levels in NSCs, NPCs, and neurons. Among the six catalytic subunits, Kmt2a/Mll1, Kmt2c/Mll3, and Kmt2d/Mll4 are expressed at high levels, while Kmt2b/Mll2, Setd1a, and Setd1b are expressed at low levels, in NSCs, NPCs, and neurons (Supplementary Figure S1B). Dpy30 is thus the only subunit of the Set1/Mll complexes that is preferentially expressed at a high level in NSCs and NPCs, again suggesting an

important role of Dpy30 in early stages of neural development. We also performed immunofluorescence staining of Dpy30 and neuronal nuclei (NeuN), a nuclear marker protein for mature neurons. In the hippocampal dentate gyrus (DG), we detected Dpy30 expression in both mature granular neurons and cells within the subgranular zone. Dpy30 was also expressed in cells within the subventricular zone (SVZ) and adjacent neuronal layers (Supplementary Figure S1C). As the DG and SVZ are the major areas with significant neurogenesis into adulthood (Bond et al., 2015), we were prompted to pursue a functional study of Dpy30 in mammalian brain development and postnatal neurogenesis.

Dpy30 deficiency results in reduction of H3K4 methylation and failure of postnatal neurogenesis

To study the biological function of Dpy30 in postnatal neurogenesis, we used the human glial fibrillary protein (*hGFAP*)-*Cre* (Zhuo et al., 2001) to excise the floxed *Dpy30* allele in NSCs present at embryonic day 13.5 (E13.5) in the dentate, cerebellar granular cell layer, and SVZ (Han et al., 2008). To avoid potential effects from *Cre* expression, we restricted our comparisons between *hGFAP-Cre; Dpy30^{f/+}* and *hGFAP-Cre; Dpy30^{f/-}* littermates as confirmed by genotyping (Supplementary Figure S1D), hereafter referred to as control and KO, respectively. The KO mice were born at the expected Mendelian ratios and were indistinguishable from their control littermates. However, by postnatal day 5 (P5), the KO mice developed progressive but severe growth retardation (Supplementary Figure S1E and F) and ataxia (Supplementary Video S1) and died between P20 and P27. This phenotype is 100% penetrant in a total of over 200 offspring animals. Moreover, we also deleted *Dpy30* using *Nestin-Cre* (Tronche et al., 1999), whose expression starts E12.5 in cortical prepalate layer and increases during perinatal development in NSCs of the subependymal zone and in NPCs of the rostral migratory stream of newborn mice (Liang et al., 2012). The *Nestin-Cre; Dpy30^{f/-}* mice exhibited essentially identical phenotypes of growth retardation (Supplementary Figure S1G) and ataxia as the *hGFAP-Cre; Dpy30^{f/-}* mice, corroborating a requirement of Dpy30 in postnatal brain development. We have thus only used the *hGFAP-Cre; Dpy30^{f/+}* (control) and *hGFAP-Cre; Dpy30^{f/-}* (KO) littermates for the rest of this study.

While most of the brain appeared morphologically normal, the hippocampal DG showed grossly altered ultrastructure and the lateral ventricles were enlarged (Figure 1A). Moreover, KO mice show a marked reduction in cerebellar folia (Supplementary Figure S1H) and cells in the internal granular layer (IGL) (Supplementary Figure S1I). *Dpy30* mRNA levels were significantly reduced in the KO SVZ and DG (Supplementary Figure S1J). As shown by immunostaining, Dpy30 was almost completely lost in the KO SVZ, DG, and cerebellar granule cell layer (Figure 1B–D). Consistent with a role of Dpy30 in regulating all three levels of H3K4 methylation (Jiang et al., 2011), we detected a modest reduction of H3K4me1, and a significant reduction of H3K4me2 and H3K4me3, by western blotting of whole brain KO lysates (Figure 1E). Confirming

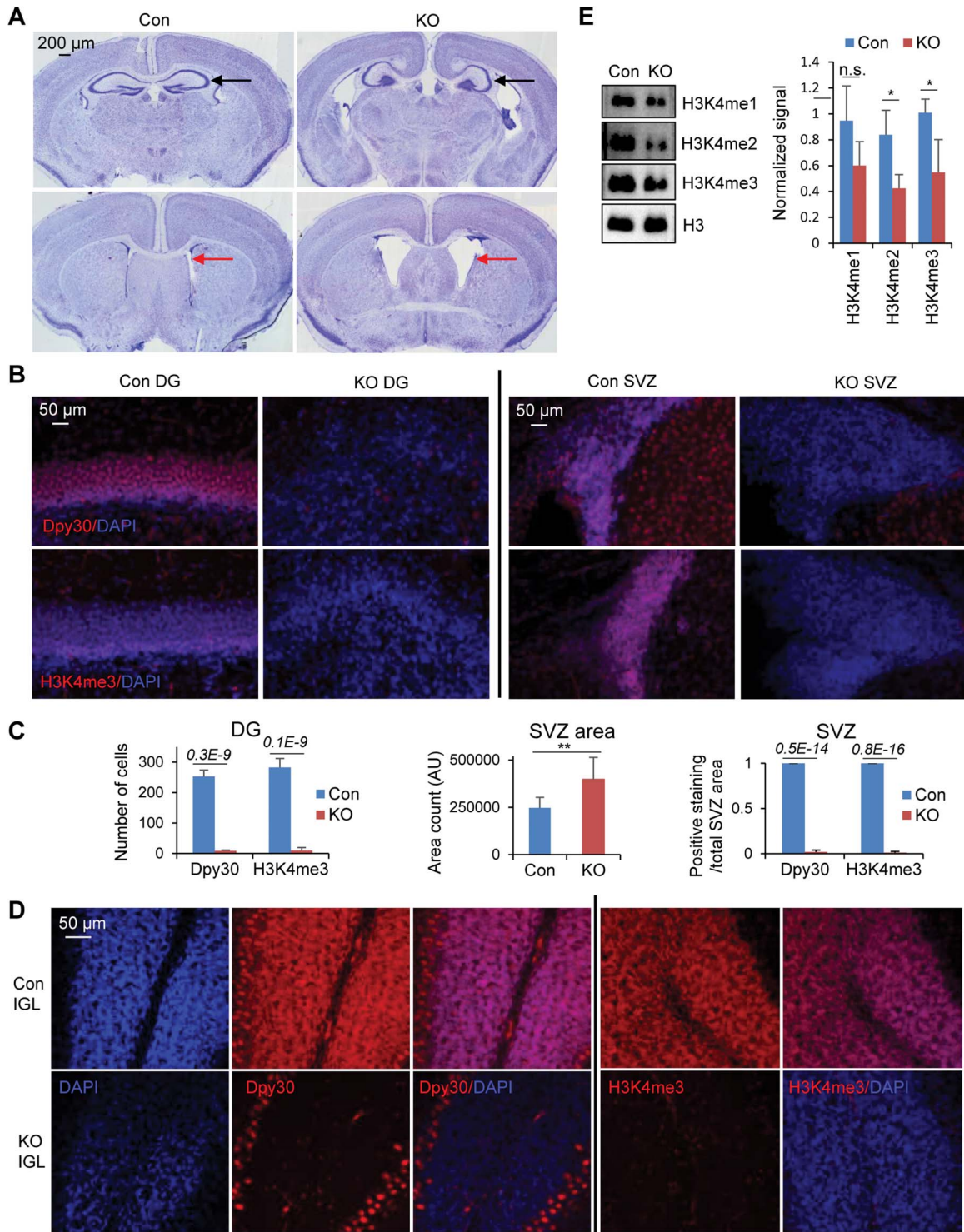


Figure 1 Dpy30 deficiency results in defective postnatal brain development. **(A)** Nissl staining of coronal sections from P12 control (Con) and KO mice. Representative of three mice each. Black arrows point to hippocampus and red arrows point to SVZ. **(B)** Staining for DAPI and Dpy30 (top) or H3K4me3 (bottom) in coronal sections from P12 control and KO mice. Representative of three mice each genotype. **(C)** Quantification of staining in **B**. **(D)** Staining for DAPI and Dpy30 (left) or H3K4me3 (right) in coronal cerebellum sections from P12 control and KO mice. Representative of three mice each genotype. IGL, internal granular layer. **(E)** H3K4 methylation levels in the whole brain lysates from P12 control and KO mice were determined by western blotting. Shown are representative results (left) and quantifications for the band intensity relative to the total H3 band intensity of the same sample (right). $n = 4$ mice each genotype. Data represent the mean \pm SD for **C** and **E**. P -values are either labeled on top of the bars or $*P < 0.05$ and $**P < 0.01$, by two-tailed Student's t -test.

this result visually, immunohistochemistry shows a stark decline in H3K4me3 staining in the DG, SVZ, as well as the cerebellar granule cells of the KO brain, compared to the control (Figure 1B–D). These results suggest an important role of Dpy30 and efficient H3K4 methylation in postnatal neurogenesis.

Transcriptome analyses suggest a requirement of Dpy30 for NSPC fate determination

To begin to understand the alterations caused by Dpy30 loss at the molecular level, we examined the gene expression profiles of micro-dissected hippocampal (containing DG) and SVZ tissues extracted from three different P12 mice of each genotype via RNA sequencing (RNA-Seq) (Supplementary Tables S1 and S2). Our Gene Ontology (GO) analysis showed that the top 10 most significantly over-represented gene functions downregulated in the KO hippocampus were involved in neuronal activities, such as synapse and ion channel activities (Supplementary Figure S2A, top left). Gene Set Enrichment Analysis (GSEA) (Subramanian et al., 2005) also revealed significant enrichment of neuronal markers (Lein et al., 2007) among genes downregulated in the KO hippocampus (Figure 2A, left), which was confirmed by quantitative PCR for the top group of neuronal markers (Supplementary Figure S2B and C). Additionally, some neuronal genes that are not included in the gene set for neuronal markers were also downregulated by Dpy30 loss in the hippocampus. For example, glutamate ionotropic receptor NMDA type subunit 2C (*Grin2c*), a neuronal specific gene (Gupta et al., 2016), was among the top 50 downregulated genes in KO hippocampus (Supplementary Figure S2E, left) and also shown by qPCR to be largely downregulated (Supplementary Figure S2C). Enrichment (but not statistically significant) of astrocytic markers (Lein et al., 2007) was also observed in genes downregulated in the KO hippocampus (Supplementary Figure S2D). These results suggest a relatively selective loss of neurogenesis and/or neuronal function in the Dpy30-deficient hippocampus.

On the other hand, the most enriched gene functions downregulated in the KO SVZ were not in mature neuronal activities, but rather included mostly GTPase regulator activities (Supplementary Figure S2A, bottom left), which are known to regulate migration of neuronal precursors and neurite outgrowth (Govek et al., 2005; Villarroel-Campos et al., 2014). Immature neurons/neuroblasts within SVZ travel from SVZ to the olfactory bulb via the rostral migratory stream and differentiate during that process (Luskin, 1993; Lois and Alvarez-Buylla, 1994). Indeed, GSEA showed that genes associated with neuroblast migration were significantly enriched among downregulated genes in the KO SVZ, but not in the KO hippocampus (Supplementary Figure S2D). These results suggest a defective precursor migration from SVZ to the olfactory bulb for differentiation. Unlike the downregulation of neuronal genes in the KO hippocampus, GSEA showed that astrocytic markers (Lein et al., 2007) were significantly enriched in genes downregulated

in the KO SVZ (Figure 2A, right), which was confirmed by qPCR for the top group of astrocytic markers (Supplementary Figure S2B and C). Again, some astrocytic markers not included in the gene set were also downregulated in the KO SVZ. For example, solute carrier family 15 member (*Slc15a2*), a gene selectively expressed in astrocytes (Lovatt et al., 2007), was among the top 50 most downregulated genes in the KO SVZ (Supplementary Figure S2E, right). *S100B* is another gene that is also specifically expressed in astrocytes (Ciccarelli et al., 1999). qPCR assays confirmed the significant downregulation of *Slc15a2* and *S100B* in the KO SVZ (Supplementary Figure S2C). We found no significant change in neuronal markers upon Dpy30 loss in SVZ (Supplementary Figure S2D). These results thus suggest a relatively specific disruption of gliogenesis in the Dpy30-deficient SVZ.

Interestingly, the top enriched gene functions upregulated upon Dpy30 loss in the KO hippocampus and those in the KO SVZ both included mostly ribosomal genes (Supplementary Figure S2A, right two panels), suggesting an increase in protein synthesis activity in these NSC-related tissues. GSEA also revealed upregulation of activated NSC gene signatures (Codega et al., 2014) in the KO hippocampus, including genes associated with protein metabolism, mRNA metabolism, and DNA repair (Supplementary Figure S2F). GSEA for the KO SVZ showed downregulation of pathways enriched in quiescent stem cells (Codega et al., 2014), such as lipid metabolism, growth factor activity, and peroxisome proliferator-activated receptor signaling (Supplementary Figure S2G). These results suggest that Dpy30 may regulate the pool of quiescent NSCs in the major postnatal neurogenic regions in brain.

By performing GSEA using a gene set upregulated at prenatal, neonatal, and postnatal stages of the mouse hippocampus (Mody et al., 2001), we found enrichment of genes characteristic for prenatal hippocampus in those upregulated in the KO hippocampus and genes for postnatal hippocampus in those downregulated in the KO hippocampus (Figure 2B). For example, aldolase, fructose-bisphosphate C (*Aldoc*), a gene selectively expressed in the postnatal hippocampus (Buono et al., 2004), was among the top 50 downregulated genes in KO hippocampus (Supplementary Figure S2E, left) and its significant downregulation was also shown by qPCR (Supplementary Figure S2C). In other words, the gene expression program of the P12 Dpy30-deficient hippocampus resembled a prenatal stage rather than a normal postnatal stage, strongly suggesting a developmental arrest of the Dpy30-deficient hippocampus. Finally, while a NSC-specific signature gene set is not readily available for GSEA, our qPCR assays showed that *Prominin1* (*Prom1*) and *Gfap*, whose coincident expression marks adult NSCs *in vivo* (Beckervordersandforth et al., 2010), were both significantly downregulated in the KO SVZ (Supplementary Figure S2C). Although our assays do not provide information on co-expression of both markers in the same cell and *Gfap* downregulation is likely a result of reduced gliogenesis, this is consistent with a reduced NSC pool or activity in the KO SVZ.

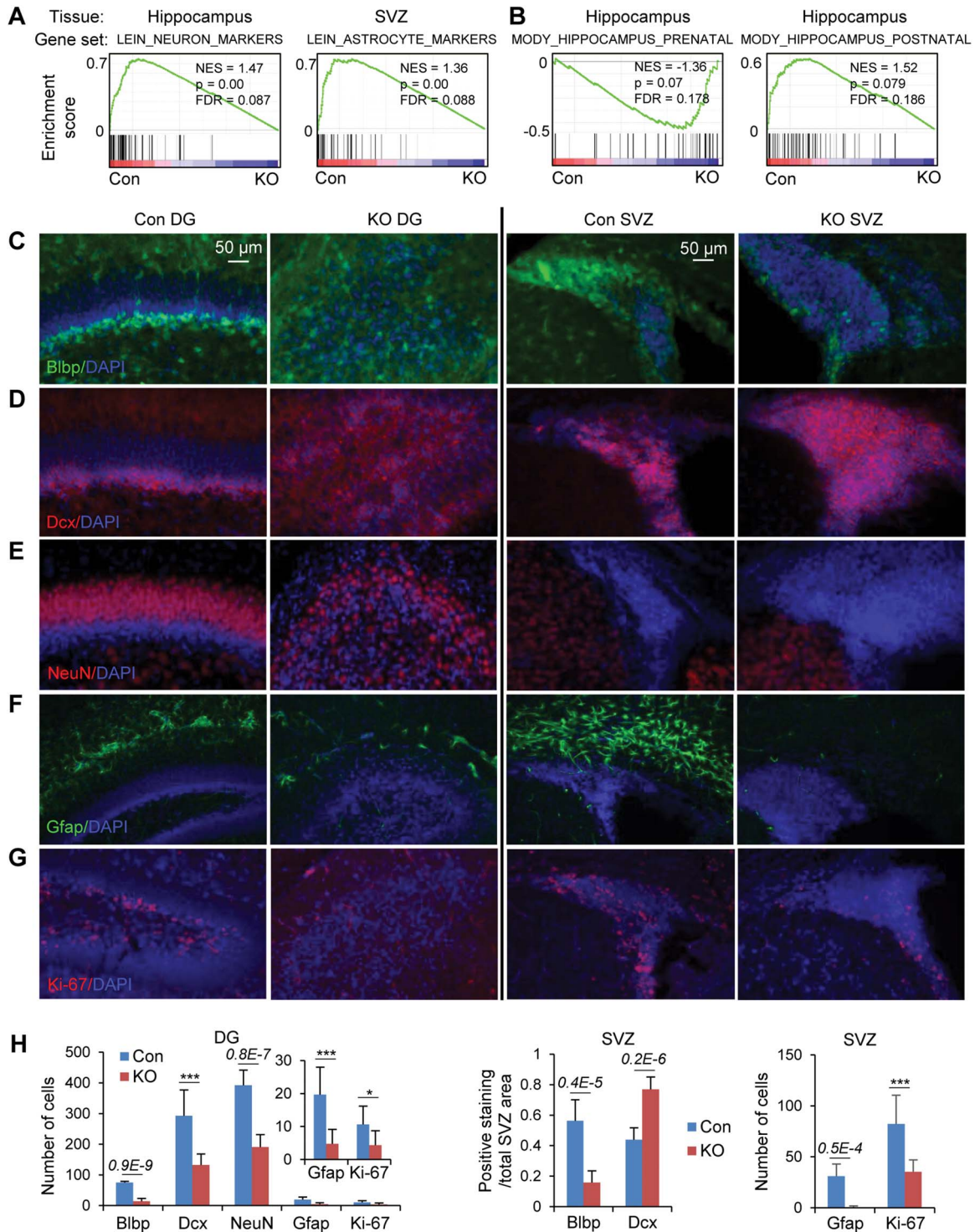


Figure 2 Dpy30 deficiency impairs neurogenesis and gliogenesis in the postnatal brain. **(A and B)** GSEA for RNA-seq results from hippocampus or SVZ cells (indicated) of P12 control and KO mice ($n = 3$ mice each) using indicated gene sets. NES, normalized enrichment score. **(C–G)** Staining for DAPI and Blbp **(C)**, Dcx **(D)**, NeuN **(E)**, Gfap **(F)**, Ki-67 **(G)** in coronal sections from P12 control and KO mice. Representative of three mice each genotype. **(H)** Quantifications of positive stained cells or area of the images in **C–G**. Both top and bottom subgranular zone/granular zone layers of the dentate were counted for control and the whole dentate (absence of a subgranular zone) was counted for KO. For SVZ, ImageJ software’s ‘area count’ was used to obtain area of positive staining and total area of SVZ. $n = 9$ (three mice, each with three different bregma levels). Data represent the mean \pm SD in **H**. P -values are either labeled on top of the bars or $*P < 0.05$, $**P < 0.01$, and $***P < 0.001$, by two-tailed Student’s t -test.

Dpy30 deficiency impairs neurogenesis and gliogenesis in the postnatal brain

The transcriptome data prompted us to further investigate the effect of Dpy30 loss on NSC activity in the developing brain, especially DG and SVZ. NSCs in both regions express brain lipid binding protein (Blbp). Consistent with the downregulation of NSC marker *Prom1* in the KO SVZ, the Blbp-expressing cell population was significantly reduced in the KO DG and SVZ compared to their corresponding control tissues (Figure 2C and H). KO DG exhibited reduced immature and mature neuronal populations as seen by doublecortin (Dcx) and NeuN staining, respectively (Figure 2D and E, left, and H). Most striking, however, is the extreme disruption of dentate morphology for both cell groups where it is impossible to distinguish distinct granular and subgranular zones. This is consistent with the reduction of neuronal markers in the KO hippocampal transcriptome. DG also showed a significant decrease in Gfap-expressing astrocyte population (Figure 2F, left). Due to differences in cellular composition around the two neurogenic regions (Ming and Song, 2011), SVZ and DG appeared to respond differently to Dpy30 loss. P12 KO SVZ exhibited accumulation of immature neurons as seen by increased Dcx staining (Figure 2D, right, and H, middle). Considering the significant downregulation of genes associated with neuroblast migration shown by the transcriptome analyses above, these results are most consistent with a disruption of neuroblast differentiation and/or migration, leading to immature neuron accumulation in the KO SVZ. Additionally, the KO SVZ showed a drastic reduction in the astrocyte population as seen by staining for Gfap (Figure 2F, right, and H, right), consistent with the enrichment of astrocytic markers among genes downregulated in the KO SVZ.

Finally, we found that the KO DG and SVZ had significantly less number of actively dividing cells expressing proliferation protein Ki-67 (Figure 2G and H) (Scholzen and Gerdes, 2000), which is also functionally crucial for cell division (Cuylen et al., 2016). Therefore, Dpy30 is required to generate or maintain the pool of proliferative NSCs. The cyclin-dependent kinase (CDK) inhibitors, such as *Cdkn1a* (p21) (Kippin et al., 2005), *Cdkn1b* (p27) (Qiu et al., 2009), and *Cdkn1c* (p57) (Furutachi et al., 2013), have been reported to constrain the proliferation of NSCs. Analysis of our RNA-seq data from the control and KO hippocampal and SVZ tissues showed that both *Cdkn1a* and *Cdkn1c* were greatly unregulated in SVZ of two out of three KO mice. While *Cdkn1c* was also upregulated in KO hippocampus, *Cdkn1a* was not (Supplementary Figure S2I). The upregulation of CDK inhibitors were selective, as *Cdkn1b* (p27) was not noticeably upregulated in either SVZ or hippocampus of the KO mice (Supplementary Figure S2I). These data are consistent with our studies showing a dramatic increase in *Cdkn1a* expression in *Dpy30* KO hematopoietic stem cells, which partially contributes to the functional defect of the KO stem cells (our unpublished data). These results further strengthen the proliferation defect of the KO NSCs and suggest that upregulation of CDK inhibitors is a general pathway in mediating reduction in proliferation of tissue-

specific stem cells upon impaired epigenetic modifications following Dpy30 loss.

Dpy30 is required for sustaining self-renewal and proliferation of NSPCs in vitro

To determine whether Dpy30 is cell-intrinsically required for self-renewal of NSCs, we extracted NSCs from SVZ of KO mice and measured their self-renewal using the neurosphere serial re-plating assay (Figure 3A) (Molofsky et al., 2003; Pastrana et al., 2011). We first confirmed our technical ability to isolate and grow multipotent control neurospheres. Control neurospheres differentiated into both neuronal and glial lineages with characteristic cell morphologies and lineage markers upon appropriate treatment (Figure 3B; Supplementary Figure S3A). However, the KO neurospheres showed low viability that precluded further analysis. Serial re-plating assays of the KO cells showed a significant reduction in both the number and size of neurospheres compared to the control cells in each passages (Figure 3C and D), and unlike controls, there were no live cells in the KO culture after the 5th passage (Figure 3C and D). Experiments to model self-renewal of hippocampal DG-derived NSCs were impossible as the cultures of the KO hippocampal tissues produced no viable cells (Supplementary Figure S3B). These results indicate that Dpy30 is required for NSCs self-renewal and/or NPCs proliferation in a cell-autonomous manner. In particular, the progressive increase in clonogenicity loss of the KO SVZ cells along each round of re-plating (Figure 3D, middle) argues that the effect was not merely an accumulated result of Dpy30 loss since the embryonic stage, but rather an intrinsic defect in self-renewal as a result of Dpy30 loss in the assayed cells.

To test the broader requirement of Dpy30 activity for NSPC activity and further address if the effects on neurogenesis only reflect an accumulated impact of Dpy30 loss, we sought to use shRNAs to acutely deplete Dpy30 from NE-4C, a mouse NPC line, and ReNcell VM, a human NPC line in culture. Dpy30 knockdown (KD) in these cells drastically decreased their ability to grow in culture (Figure 3E). Moreover, percentage of the Ki-67-positive cells was also significantly reduced by Dpy30 KD in these cells (Figure 3F). This suggests that Dpy30 is required for maintaining the NSPC proliferation.

Dpy30 directly regulates differentiation of NPCs to neuronal and glial lineages

We next studied the effect of Dpy30 KD on differentiation of these cultured NPCs. Upon treatment of differentiation conditions, while the control mouse NPCs differentiated into cells positive for β -Tubulin III (Tuj1) with extensive fiber-containing morphology representing neuronal axons, the Dpy30-KD mouse NPCs failed to produce any cells positive for β -Tubulin III or with fiber-like structure (Figure 4A; Supplementary Figure S4A). We were unable to determine the effect on their glial differentiation as the control mouse NPCs also did not differentiate to glial lineages (data not shown). Dpy30 KD in the human NPCs

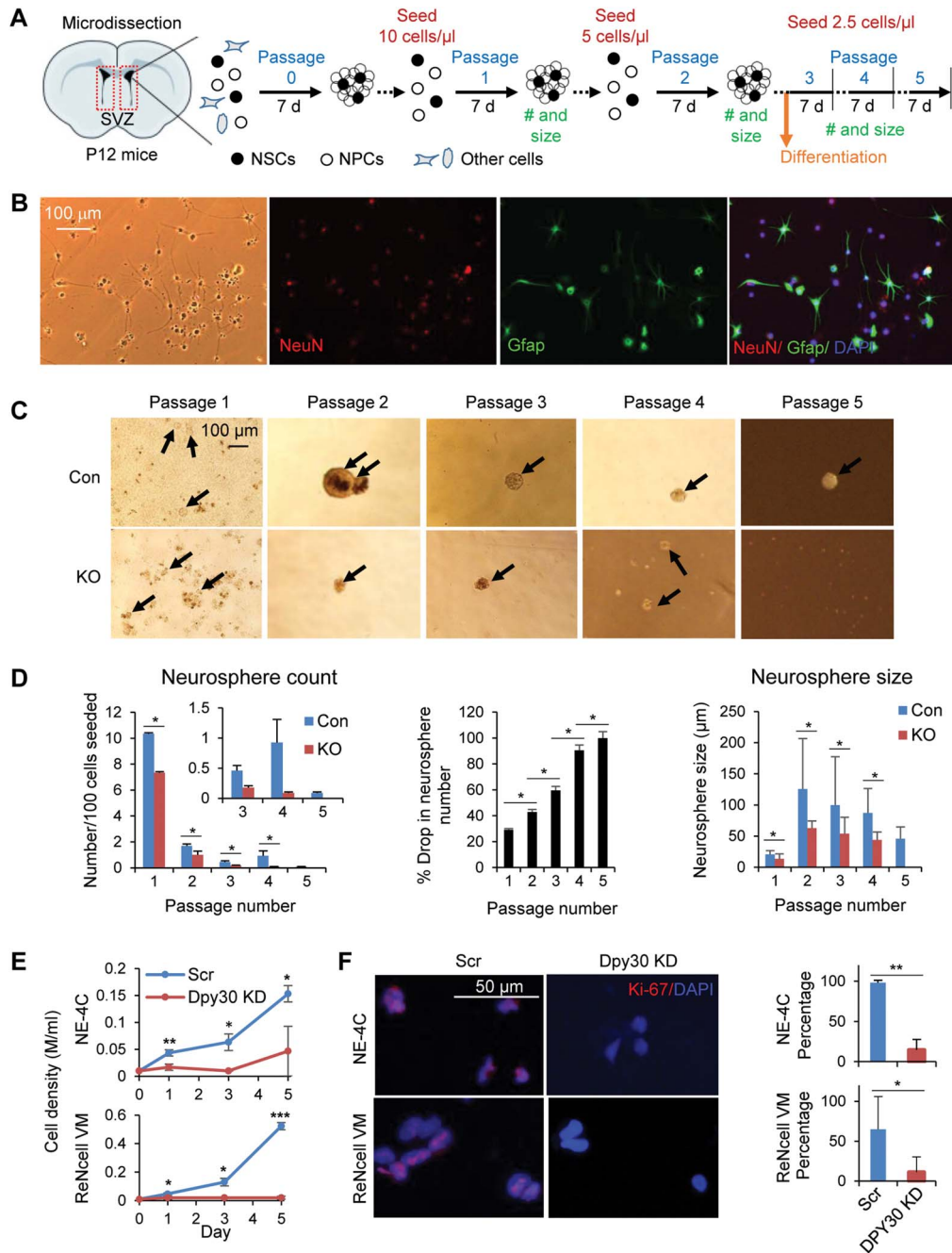


Figure 3 Dpy30 is required for sustaining the self-renewal and proliferation of NSPCs. **(A)** Diagram for the neurosphere assays including serial re-plating and differentiation. **(B)** Images of differentiated neurospheres obtained from SVZ of control mice. NeuN for neurons and Gfap for glia. Representative of three control mice. **(C)** Serial re-plating assay with NSCs isolated from SVZ of control and KO mice. Representative of two mice each. Images were taken 7 days into the indicated passage (top) except passages 1 and 4, which were taken 5 days into the passage. **(D)** Quantifications of number of neurospheres per 100 cells seeded (left), percent drop in neurosphere number (middle), and neurosphere size (right) at each passage. $n = 2$ mice each genotype. Percent drop was calculated as $(\text{control count} - \text{KO count}) / \text{control count} \times 100\%$ at each passage. Neurosphere size was calculated by measuring the diameters of multiple neurospheres from two mice each genotype. Total measured neurosphere number $n = 50$ for each genotype at passage 1, $n = 39$ (control) or 6 (KO) at passage 2, $n = 46$ (control) or 18 (KO) at passage 3, $n = 93$ (control) or 8 (KO) at passage 4, and $n = 9$ (control) at passage 5. There was no KO neurosphere in passage 5. **(E and F)** Growth assays **(E)** and staining for Ki-67 and DAPI **(F)** for stably selected control (Scr) and Dpy30-KD NE-4C mouse NPCs (top) and ReNcell VM human NPCs (bottom). Shown in **F** are representative images (left) and quantifications (right). $n = 3$ independent infections for all. Data represent the mean \pm SD for **D–F**. $*P < 0.05$, $**P < 0.01$, $***P < 0.001$, by Mann–Whitney U test ($\alpha = 0.05$) for middle and left panels in **D**, and two-tailed Student’s t -test for **D** (right panel), **E**, and **F**.

clearly abolished their glial differentiation as shown by the extensive GFAP-positive cells from differentiation of the control NPCs but the drastic reduction of the number and percentage of these cells from the DPY30-KD NPCs (Figures 4D and E; Supplementary Figure S4B). Regarding neuronal differentiation of the human NPCs, while we detected significantly lower number of the NEUN-positive cells for the DPY30-KD compared to the control cells after providing differentiation conditions (Figure 4D; Supplementary Figure S4B), the percentage of NEUN-positive cells was not significantly different between control and KD due to the lower number of the overall KD cells (Figure 4E; Supplementary Figure S4B). However, even with the greatly underestimated quantification of the fibers in the differentiated control cells (due to their extensively intertwined structures), we found that the KD cells gave rise to significantly lower percentage of cells with long fibers/processes characteristic of neuronal axons (Figure 4E; Supplementary Figure S4B, bottom). These results suggest inefficient neuronal differentiation of the human NPCs upon DPY30 KD. We also examined the effect of depletion of ASH2L, the direct interaction partner of DPY30 and also a core subunit of the SET1/MLL complexes (Cho et al., 2007) in human NPCs. While we were able to achieve ~50% KD efficiency before differentiation, the KD efficiency became very low after treatment of differentiation conditions (Supplementary Figure S4C), suggesting that cells with efficient ASH2L depletion were incompatible with the differentiation conditions and likely selected against during the process.

To further understand the differentiation defect of Dpy30-KD mouse and human NPCs, we analyzed the expression change of a number of genes known to regulate NSC or NPC fate determination. These genes include *NEUROD1* (Boutin et al., 2010) and *NEUROG1* (Sun et al., 2001), which encode E-box-binding transcriptional activators critical for neuronal differentiation, and *MAP2*, which encodes a cytoskeletal protein determining and stabilizing dendritic shape during neuron development (Harada et al., 2002). We did not find downregulation of some of these genes in the micro-dissected *Dpy30* KO hippocampal or SVZ tissues (Supplementary Figure S2C), and suspected that contamination of Dpy30-intact cells may contribute to the lack of downregulation, and thus sought to investigate these genes in the much more homogenous cell lines in culture. These genes were induced after differentiation in the control cells but failed to be induced under the same differentiation conditions in the mouse and human NPCs depleted of Dpy30 (Figure 4B and F). We also examined the expression change of genes involved in gliogenesis such as *GFAP* and *S100B*. Similar to the effect on the neurogenic genes, *GFAP* expression was elevated upon differentiation of control NPCs, but such induction was significantly impaired or completely lost in NPCs depleted of Dpy30 (Figure 4B and F). The expression of *S100B* was significantly reduced by DPY30 KD before differentiation, and this reduction became more prominent after differentiation of the human NPCs (Figure 4F). Even in the cells that started with decent but ended with minimal depletion of ASH2L under the differentiation conditions, the

expression of both the neurogenic and gliogenic genes was modestly impaired compared to the control at the end of the differentiation process (Supplementary Figure S4C). These results indicate a requirement of the H3K4 methyltransferase complexes in efficient expression of the lineage specification genes during NPC fate determination.

As shown by chromatin immunoprecipitation (ChIP) assays, Dpy30 bound to the transcriptional start sites of these genes (Figure 4C and G, top; Supplementary Figure S4D and E, top) in at least one of the NPC models, suggesting that Dpy30 directly controls the expression of these key neurogenesis genes. As a consequence of reduced Dpy30 binding to these genes upon Dpy30 KD, H3K4me3 was reduced at many of these genes (Figure 4C and G, bottom; Supplementary Figure S4D and E, bottom) except *Gfap/GFAP* (see Discussion). These results further support a direct and cell-intrinsic role of Dpy30 and its associated H3K4 methylation in the fate determination of neural stem and progenitor cells.

Discussion

Our results from both *in vivo* and *in vitro* assays strongly suggest a requirement of Dpy30 for the self-renewal and differentiation of NSCs in a cell-intrinsic manner. NSCs in DG and SVZ are significantly reduced upon loss of Dpy30. Cells extracted from the KO DG were unable to form neurospheres *in vitro*. Although the cells from the KO SVZ were able to form neurospheres *in vitro*, the serial replating assays clearly showed a gradually increased loss of neurospheres along each round of replating of the same number of cells from the KO SVZ. Consistent with the reduction of Ki-67-positive cells in the KO DG and SVZ, acute depletion of Dpy30 in human or mouse NPCs greatly reduced their growth and Ki-67 expression, further supporting a requirement of Dpy30 in NSPC proliferation. Although not examined in this work, increase in apoptosis may also contribute to the reduction in viability upon Dpy30 loss in NPCs. DPY30 and ASH2L also enable the differentiation capacity of NPCs to both neuronal and glial lineages by directly regulating the epigenetic modifications of key genes in these pathways. This is consistent with a requirement of Dpy30 and Rbbp5 for the neuronal differentiation from ESCs (Jiang et al., 2011), where these H3K4 methylation modulators epigenetically prime the bivalently marked lineage-specific genes for efficient induction upon differentiation cues.

A few lines of evidence support that the phenotypic defects of the Dpy30 KO brain are at least partially due to postnatal loss of Dpy30, including our *in vitro* neurosphere assays that revealed intrinsic defects along serial re-plating of the postnatal brain tissues, and the profound reduction of cells in the IGL of cerebellum (Supplementary Figure S1), which is known to be postnatally generated. However, considering the high expression of Dpy30 at hippocampus and cerebellum at both the late embryonic and postnatal stages (Supplementary Figure S1A), Dpy30 most likely regulates both of these stages of neural system development, and the *in vivo* defects are probably a combined result of Dpy30 loss in both of these stages.

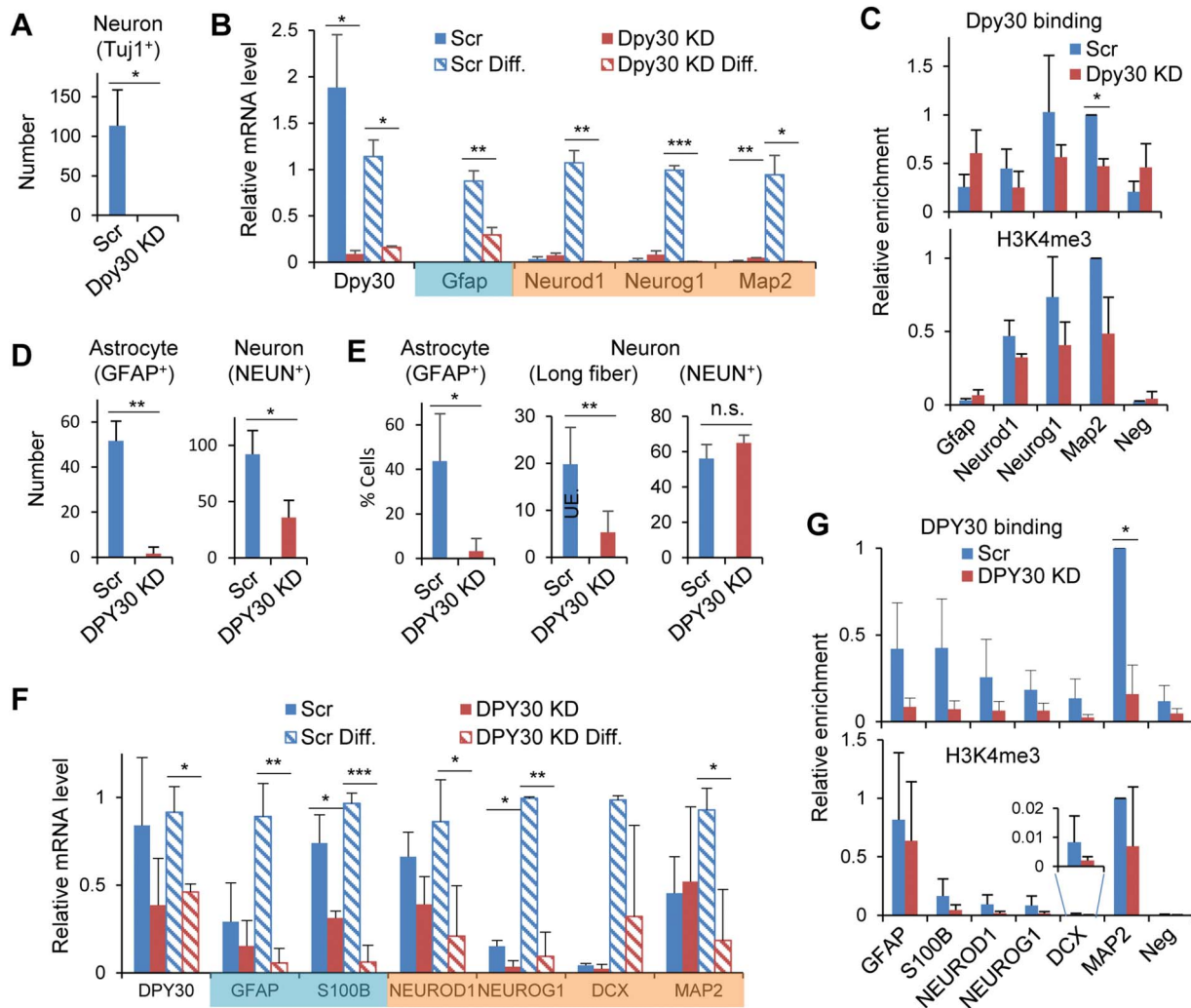


Figure 4 Dpy30 directly regulates NPC differentiation and induction of key genes for differentiation. **(A and B)** Differentiation of NE-4C mouse NPCs. $n = 3$ biological repeats. **(D–F)** Differentiation of ReNcell VM human NPCs. $n = 3$ biological repeats. **(A and D)** Number of neurons and astrocytes (indicated) found in the control and KD culture after 9 days of differentiation. For **A**, a percentage plot was not possible due to extensively overlapping DAPI-positive cells in control (Scr) culture. As no Tuj1-positive cells were seen in KD culture, the conclusion based on cell number would be in agreement with percent cell calculations. Scr, scrambled control shRNA. Neurons were identified based on Tuj1 (for mouse) or NEUN (for human) staining, and astrocytes based on GFAP staining. **(E)** Percent astrocytes and neurons found in Scr and DPY30-KD ReNcell VM human NPCs after 9 days of differentiation. Astrocytes were identified based on GFAP staining. Neurons were identified based on long ($> 20 \mu\text{m}$) fibers or NEUN staining. The plots show the percentage of the number of cells with indicated characteristics in the total number of DAPI-positive cells. UE, underestimated, due to extensively intertwined structure. **(B and F)** Relative mRNA levels were determined by qPCR and normalized to *Gapdh/GAPDH* for indicated genes upon *Dpy30/DPY30* KD with and without treatment of differentiation conditions for 9 days in NE-4C **(B)** or ReNcell VM **(F)** cells. One of the biological repeats for ‘Scr Differentiated’ was set to one for each gene. Gene names are shaded in aqua for gliogenesis and in orange for neurogenesis. **(C and G)** Dpy30 and H3K4me3 ChIP-qPCR in NE-4C **(C)** or ReNcell VM **(G)** cells. Relative enrichment was generated by calculating percent input for each locus followed by normalizing to the percent input for the *Map2/MAP2* locus in the control cells. Data represent the mean \pm SD. Two factor ANOVA analysis followed with post hoc *t*-test was performed in **B** and **F**. * $P < 0.05$, ** $P < 0.01$, and *** $P < 0.001$, by two-tailed Student’s *t*-test for the rest of the figure.

Our gene profiling results also support a developmental arrest of the hippocampus upon Dpy30 loss and begin to reveal molecular pathways governed by Dpy30 and H3K4 methylation in postnatal neuronal and glial development. Due to the technical difficulty of extracting pure cell populations and the high heterogeneity of the tissues in DG and SVZ, our gene

profiling results from pooled cells do not necessarily show gene expression changes in NSCs, but most likely also reflect changes of cellular composition. Either interpretation supports halted development of hippocampus and gliogenesis in SVZ following loss of Dpy30 and H3K4 methylation. Moreover, the impure cell populations could mask changes of expression of certain genes,

such as *Neurod1* and *Neurog1* (Supplementary Figure S2C), which are directly regulated by Dpy30 for efficient induction in the much more homogenous NPC lines (Figure 4B, C, F, and G). Alternatively, these genes may be robustly regulated *in vivo* through other mechanisms that were not active in the cultured cells. While we have shown the significant change in expression of a number of neurogenesis genes in DG and SVZ of the KO brains, we note that the strong cellular phenotypes may not necessarily arise from significant changes in expression levels of individual genes. Chromatin modulators such as Dpy30 globally (but not uniformly) influence the genome compaction and accessibility, and the collective effects from subtle changes in numerous genes may result in significant cellular phenotypes.

Dpy30 was originally discovered as a gene required for dosage compensation and development of *Caenorhabditis elegans*. Dpy30 mutations cause complete lethality in XX *C. elegans* and numerous abnormalities in XO animals including uncoordinated movement (Hsu and Meyer, 1994), suggesting a requirement of Dpy30 for neuromuscular development. Here, we show that loss of Dpy30 in neurogenic regions (including the cerebellar cells) of the brain results in ataxia like uncoordinated movement in these mice. The deficiency of Dpy30 and H3K4 methylation in the KO cerebellum suggests a direct role of this epigenetic modification in cerebellar development.

Conditional deletion of *Mll1* (Lim et al., 2009) or *Dpy30* by the same *hGFAP-Cre* results in partially similar phenotypes yet with important differences. The physiological phenotypes following loss of *Mll1* or *Dpy30* are highly similar, and include ataxia, postnatal growth retardation and death around P25–P30 (for *Mll1*) or P20–P27 (for *Dpy30*). The effects on the brain ultrastructure are also similar with hypocellular DG and expanded SVZ. However, important differences are revealed at cellular and molecular levels. While *Mll1* is important for neurogenesis but not gliogenesis, *Dpy30* is important for NPC differentiation to both lineages in a cell-intrinsic manner. NSC self-renewal was not examined for *Mll1* KO, but the unaffected gliogenesis suggest that NSC maintenance is probably unaffected by *Mll1* loss (Lim et al., 2009). *Dpy30*, however, appears to be required for the self-renewal capacity of NSCs *in vivo* and *in vitro*. At the molecular level, *Mll1* loss leads to reduced expression *Dlx2* and *Mash1* without alteration of local H3K4 methylation. *Dpy30* loss, however, profoundly impaired the induction potential of several crucial genes in neurogenesis, accompanied by dramatic loss of global H3K4 methylation and modest reduction of H3K4me3 at affected genes. We detected a significant reduction in DPY30 binding, but not in H3K4me3, at the *GFAP* transcription start site upon DPY30 KD in the ReNcell VM human NPCs (Figure 4G; Supplementary Figure S4E). Based on the dependence of H3K4me3 on Dpy30 at the biochemical and genomic levels (Jiang et al., 2011), we surmise that a reduction of H3K4me3 could be at a different site that would be shown by sequencing but not a single-point qPCR assay. Alternatively, we cannot rule out the possibility that other

activities of DPY30 may be responsible for its regulation of GFAP expression.

These results highlight a complex relationship between the enzymatic and non-enzymatic activities of the subunits in the histone modification writer complexes. The important roles of *Mll1* in regulating hematopoietic stem cells, leukemogenesis, and neurogenesis do not require its H3K4 methylation activity and are most likely mediated by its interaction with other proteins (Lim et al., 2009; Mishra et al., 2014). *Dpy30*, being a core and common subunit of all six Set1/*Mll* complexes, is indispensable for efficient H3K4 methylation throughout the genome. Moreover, depletion of *ASH2L*, another common core subunit of all SET1/*MLL* complexes, also affected the expression of neurogenic and gliogenic genes upon treatment of differentiation conditions in the NPCs. Therefore, *Dpy30* regulates NSC function most likely, or at least partially, through interacting with *Ash2l* and regulating the H3K4 methylation activity of one or more of the Set1/*Mll* subunits. In this regard, it is interesting to see the different expression pattern of the individual core and catalytic subunit of the Set1/*Mll* complexes at a single cell level (Supplementary Figure S1B). Being the only core subunit that is preferentially expressed at NSPCs compared to their progeny, *Dpy30* may hold a special position in regulating NSPC activities. In addition to the Set1/*Mll* complex components as the major associated proteins, *Dpy30* also associates with a few other proteins including the NURF chromatin-remodeling complexes and AKAP95 (Jiang et al., 2013; Tremblay et al., 2014). We thus cannot exclude a role of *Dpy30* in NSC regulation through interacting with these factors.

In summary, by using both genetic inactivation in mouse and *in vitro* assays, our studies uncover a profound requirement of *Dpy30* and its associated H3K4 methylation in sustaining the functionality of NSCs through regulating both the self-renewal and lineage differentiation capacities. This knowledge may have implications in neurodevelopmental disorders associated with mutations in the writers, erasers, and readers of H3K4 methylation.

Materials and methods

Animals

All animal procedures were approved by the Institutional Animal Care and Use Committee at the University of Alabama at Birmingham. *hGFAP-Cre* mouse (JAX #004600) and *Nestin-Cre* mouse (JAX #003771) were obtained from the Jackson Laboratory. *Dpy30*^{+/-} and *Dpy30*^{F/F} mice were previously generated in our laboratory (Yang et al., 2016). *hGFAP-Cre* mice were crossed with *Dpy30*^{+/-} mice to obtain *hGFAP-Cre; Dpy30*^{+/-} mice. The latter were then crossed with *Dpy30*^{F/F} mice to obtain *hGFAP-Cre; Dpy30*^{F/+} (Control) and *hGFAP-Cre; Dpy30*^{F/-} (KO) from the same litter. KO mice die naturally around 20–27 days after birth and thus the brains were harvested before 15 days old. Both male and female mice were utilized.

Tissue preparation, immunofluorescence staining, imaging, and quantification

Tissue was harvested and placed in 4% paraformaldehyde for 48 h at 4°C. Serial 40 µm, free-floating coronal sections from different bregma levels (together representing 1/6 of the brain) were generated for each immunostaining. These sections were permeabilized in Tris-buffered saline containing TritonX-100 (TBST; 50 mM Tris with 0.9% NaCl, 0.5% TritonX-100) for 10 min, incubated with 0.3% H₂O₂ for 10 min, and blocked with 10% goat serum/TBST for 30 min at room temperature. Primary antibodies were incubated in 1% goat serum/TBST for 48 h rocking at room temperature. Primary antibodies for Dpy30 (Jiang et al., 2011), H3K4me3 (1:500, Millipore MP 07-473), Ki-67 (1:500, Abcam, ab15580), Blbp (1:300, Millipore, ABN14), Dcx (1:200, Abcam, ab18723), Gfap (1:500, Cell Signaling, 3670S), NeuN (1:300, Millipore, ABN78), and β-Tubulin III (Tuj1, 1:1000, Biolegend, 802001) were used. All primary antibodies are of rabbit host except Gfap, which was of mouse host. Secondary antibodies conjugated to Alexa 488 or 546, or 568 (Biolegend) were used. The sections were incubated in 1% goat serum/TBST for 4 h each sequentially in 1:500 dilution of secondary antibodies. Nuclei were labeled with 4',6-diamidino-2-phenylindole (DAPI, Life Technologies) and mounted in Fluoro Care Anti-Fade mounting media (Bicore Medical, FP001G10) on 1% gelatin-coated microscope slides (Fisher Scientific, 12-550-15). For certain double immunostaining assays where both primary antibodies are from the same species, a sequential staining was performed with excessive washing in between. For Nissl stain, after mounting free-floating sections on gelatin-coated slides, sections were incubated with 1% cresyl violet acetate, washed with dH₂O and dehydrated with graded ethanol and xylenes.

All images were collected with an Olympus BX53 fluorescent microscope with DP72 camera. For *in vivo* cell population and proliferation quantification, the average total number of indicated staining cells was manually counted from three different sections for DG and SVZ each from one mouse. This was done for a total of three different mice for control and KO each. For quantification of all staining in DG, only cells in focus (on one plane) from both arms of DG were counted. For Dpy30 and H3K4me3, cells with a positive nuclear staining were counted. For Blbp quantification, cells with nuclear staining along with an axon-like projection were counted. For Dcx quantification, cells showing a reticulate/halo of the staining with a long process were counted. For NeuN quantification, positive nuclear staining was counted. For quantification of all SVZ staining except Gfap and Ki-67, total area and area of positive staining was measured using ImageJ 'measure tool' that provides user with an 'area count' in arbitrary units. The area of positive staining was then divided by total area of SVZ to report the ratio. For Gfap quantification, the cells right above the DG and SVZ structure showing radial tubular projection staining were counted. For Ki-67 quantification in both DG and SVZ, red dots within the DG and SVZ were counted. No NeuN was found in the SVZ of control or KO mice.

Neurosphere assays

Isolation. Progenitors were isolated from 12 days old SVZ tissue using 0.05% trypsin. Neurospheres were grown on non-tissue culture treated plates with mouse NeuroCult proliferation media (Stem Cell Technologies) containing 10 ng/ml bFGF (ProSpec), 10 ng/ml EGF (ProSpec), and 2 µg/ml heparin (Fisher Scientific). In the case of progenitors isolated from 12 days old hippocampi, cells from KO mice brain did not grow at all in culture and hence could not be used in serial re-plating or differentiation assays described below.

Serial re-plating assay. The process of the directly isolated progenitors (as explained above) in proliferation media for 7 days is defined as 'passage 0'. Neurospheres were dissociated using Accutase (Fisher Scientific). Single cell dissociation was plated in 6-well (non-tissue culture treated) plates at 20000 cells/well in 2 ml of complete proliferation media (thus 10 cells/µl). Seven days later (at passage 1) primary neurosphere number per well was counted and their diameters were measured. Following evaluation, primary neurospheres were collected, dissociated, and re-plated at 10000 cells/well (thus 5 cells/µl). Secondary sphere number and size were evaluated 7 days later (at passage 2). Secondary spheres were again dissociated and re-plated at 5000 cells/well (thus 2.5 cells/µl) for three more passages to further evaluate self-renewal. Images of neurospheres were taken on a Nikon Eclipse Ti-S inverted microscope system and the diameter of each sphere was measured manually from images using a ruler (and scale bar from images for conversion 2.5 cm = 100 µm for images taken with a 10× objective). Neurospheres at passage 0 were not characterized because of concern of non-clonality and variation in the number of the initiating cells due to variation in the amount of dissected tissue out of control and KO brain. Counting neurospheres for passages 1 and 2 was performed by sampling 100 µl of culture under microscope. The number of neurospheres counted in 100 µl of culture was then multiplied by 20 to get an estimation of total neurospheres in 2 ml media. Counting for passages 3–5 was performed from images since the neurospheres then became fewer and could be captured by multiple non-overlapping images covering the whole area of a well.

Differentiation assay. Neurospheres at passage 3 were dissociated and plated at 10000 cells/well in Poly-L-ornithine (Sigma, P3655) and Laminin (Millipore, CC095) coated plates in differentiation media (NeuroCult media without growth factors). Staining was performed as described for coronal sections in immunofluorescence protocol at 10 days in differentiation media. Images were taken as described in Serial re-plating assay.

NPC culture, gene knockdown (KD), growth, and differentiation

For stable KD, ReNcell VM (Millipore, SCC008) and NE-4C (ATCC, CRL-2925) cells were grown and maintained as recommended by the vendor's protocol. ReNcell VM is an immortalized human neuronal progenitor cell line derived from ventral mesencephalon of human fetal brain and has the ability

to readily differentiate into neurons and glia cells. NE-4C is a neuroepithelial cell line derived from cerebral vesicles of 9-day-old mouse *p53*^{-/-} embryos that differentiate into neurons upon induction with retinoic acid (Schlett and Madarasz, 1997). These cells were infected with lentiviruses expressing control or human or mouse Dpy30 shRNAs [all sequences are available in Yang et al. (2014)], or human ASH2L shRNA (5'-CCTGCTGTATGAACGGGTTT-3'), followed by selection using 2 µg/ml of puromycin (Invivogen, 58-58-2) for 2–3 days starting from 2 days after infection. Live cells were counted using Trypan blue (Gibco, 15250061) exclusion. Cells were then used for RT-qPCR analysis, ChIP-qPCR analysis, and differentiation assays.

For NPC growth assays, puromycin-selected cells were plated at 10000 cells/ml in the cell maintenance media in the absence of selecting antibiotic to exclude the possibility of altered expression of antibiotic-resistance gene, and number of live cells was counted using a hemocytometer on indicated days. For NPC differentiation assays, puromycin selected cells were plated at 100000 cells/well in a 12-well plate and maintained at 1.2 µg/ml puromycin. ReNcell VM cells were cultured in differentiation media that consists of cell maintenance media with puromycin, but without growth factors. NE-4C cells were differentiated by adding 1 µM all-trans retinoic acid (Sigma, 302-79-4) to the culture media with puromycin. After nine days into differentiation, cells were counted, harvested for RNA isolation and measurement of mRNA levels, and stained as described for coronal section staining in Immunofluorescence protocol. Quantification was performed on images taken from three independent assays. In dual staining assays, completely overlapping yellow dots were not counted. Partially overlapping yellow dots were counted as one for neuron and one for glia since these are different cells growing partially on top of each other.

RNA-seq data sets

Our RNA-seq data sets have been deposited in the Gene Expression Omnibus database under GSE114091.

Statistics

All data are reported as mean ± SD. Unless indicated otherwise in legends, unpaired and equal variance, two-tailed Student's *t*-test was used to calculate *P*-values and evaluate the statistical significance of the difference between control and KO samples in all comparisons. *F*-test was used to determine if variances are equal. *P*-value < 0.05 was considered significant. For Figure 3D left and middle panels, a Mann–Whitney *U* test was performed to evaluate the difference between control and KO neurosphere number and subsequent drop between consecutive passages at alpha 0.05. For Figure 4B, F, and Supplementary Figure S4C, all samples comparison was performed using two-factor ANOVA with replication, followed by *post hoc t*-test. **P* < 0.05, ***P* < 0.01, ****P* < 0.001, *****P* < 0.0001, and ******P* < 0.00001.

Supplementary material

Supplementary material is available at *Journal of Molecular Cell Biology* online.

Acknowledgements

We thank Zhenhua Yang for technical assistance with mouse dissection.

Funding

This work was supported by Start-up funds from the University of Alabama at Birmingham, the University of Virginia, and National Institutes of Health (NIH) grant R01DK105531. H.J. is a recipient of American Society of Hematology Scholar Award, American Cancer Society Research Scholar Grant, and The Leukemia & Lymphoma Society Scholar Award.

Conflict of interest: none declared.

Author contributions: K.S. designed and performed experiments and analyzed results. G.D.K. helped design experiments and analyze results and provided technical advice and intellectual guidance. H.J. conceived the study and designed experiments. All authors wrote the manuscript.

References

- Beckervordersandforth, R., Tripathi, P., Ninkovic, J., et al. (2010). In vivo fate mapping and expression analysis reveals molecular hallmarks of prospectively isolated adult neural stem cells. *Cell Stem Cell* 7, 744–758.
- Bond, A.M., Ming, G.L., and Song, H. (2015). Adult mammalian neural stem cells and neurogenesis: five decades later. *Cell Stem Cell* 17, 385–395.
- Boutin, C., Hardt, O., de Chevigny, A., et al. (2010). NeuroD1 induces terminal neuronal differentiation in olfactory neurogenesis. *Proc. Natl Acad. Sci. USA* 107, 1201–1206.
- Buono, P., Barbieri, O., Alfieri, A., et al. (2004). Diverse human aldolase C gene promoter regions are required to direct specific LacZ expression in the hippocampus and Purkinje cells of transgenic mice. *FEBS Lett.* 578, 337–344.
- Cho, Y.W., Hong, T., Hong, S., et al. (2007). PTIP associates with MLL3- and MLL4-containing histone H3 lysine 4 methyltransferase complex. *J. Biol. Chem.* 282, 20395–20406.
- Ciccarelli, R., Di Iorio, P., Bruno, V., et al. (1999). Activation of A(1) adenosine or mGlu3 metabotropic glutamate receptors enhances the release of nerve growth factor and S-100β protein from cultured astrocytes. *Glia* 27, 275–281.
- Codega, P., Silva-Vargas, V., Paul, A., et al. (2014). Prospective identification and purification of quiescent adult neural stem cells from their in vivo niche. *Neuron* 82, 545–559.
- Cuylen, S., Blaukopf, C., Politi, A.Z., et al. (2016). Ki-67 acts as a biological surfactant to disperse mitotic chromosomes. *Nature* 535, 308–312.
- Furutachi, S., Matsumoto, A., Nakayama, K.I., et al. (2013). p57 controls adult neural stem cell quiescence and modulates the pace of lifelong neurogenesis. *EMBO J.* 32, 970–981.
- Govek, E.E., Newey, S.E., and Van Aelst, L. (2005). The role of the Rho GTPases in neuronal development. *Genes Dev.* 19, 1–49.
- Gupta, S.C., Ravikrishnan, A., Liu, J., et al. (2016). The NMDA receptor GluN2C subunit controls cortical excitatory-inhibitory balance, neuronal oscillations and cognitive function. *Sci. Rep.* 6, 38321.

- Han, Y.G., Spassky, N., Romaguera-Ros, M., et al. (2008). Hedgehog signaling and primary cilia are required for the formation of adult neural stem cells. *Nat. Neurosci.* *11*, 277–284.
- Harada, A., Teng, J., Takei, Y., et al. (2002). MAP2 is required for dendrite elongation, PKA anchoring in dendrites, and proper PKA signal transduction. *J. Cell Biol.* *158*, 541–549.
- Hirabayashi, Y., Suzuki, N., Tsuboi, M., et al. (2009). Polycomb limits the neurogenic competence of neural precursor cells to promote astrogenic fate transition. *Neuron* *63*, 600–613.
- Hsu, D.R., and Meyer, B.J. (1994). The dpy-30 gene encodes an essential component of the *Caenorhabditis elegans* dosage compensation machinery. *Genetics* *137*, 999–1018.
- Hwang, W.W., Salinas, R.D., Siu, J.J., et al. (2014). Distinct and separable roles for EZH2 in neurogenic astroglia. *Elife* *3*, e02439.
- Jiang, H., Lu, X., Shimada, M., et al. (2013). Regulation of transcription by the MLL2 complex and MLL complex-associated AKAP95. *Nat. Struct. Mol. Biol.* *20*, 1156–1163.
- Jiang, H., Shukla, A., Wang, X., et al. (2011). Role for Dpy-30 in ES cell-fate specification by regulation of H3K4 methylation within bivalent domains. *Cell* *144*, 513–525.
- Kippin, T.E., Martens, D.J., and van der Kooy, D. (2005). p21 loss compromises the relative quiescence of forebrain stem cell proliferation leading to exhaustion of their proliferation capacity. *Genes Dev.* *19*, 756–767.
- Kouzarides, T. (2007). Chromatin modifications and their function. *Cell* *128*, 693–705.
- Laubert, S.M., Nakayama, T., Wu, X., et al. (2013). H3K4me3 interactions with TAF3 regulate preinitiation complex assembly and selective gene activation. *Cell* *152*, 1021–1036.
- Lein, E.S., Hawrylycz, M.J., Ao, N., et al. (2007). Genome-wide atlas of gene expression in the adult mouse brain. *Nature* *445*, 168–176.
- Liang, H., Hippenmeyer, S., and Ghashghaei, H.T. (2012). A nestin-cre transgenic mouse is insufficient for recombination in early embryonic neural progenitors. *Biol. Open* *1*, 1200–1203.
- Lim, D.A., and Alvarez-Buylla, A. (2014). Adult neural stem cells stake their ground. *Trends Neurosci.* *37*, 563–571.
- Lim, D.A., Huang, Y.C., Swigut, T., et al. (2009). Chromatin remodelling factor Mll1 is essential for neurogenesis from postnatal neural stem cells. *Nature* *458*, 529–533.
- Lois, C., and Alvarez-Buylla, A. (1994). Long-distance neuronal migration in the adult mammalian brain. *Science* *264*, 1145–1148.
- Lovatt, D., Sonnewald, U., Waagepetersen, H.S., et al. (2007). The transcriptome and metabolic gene signature of protoplasmic astrocytes in the adult murine cortex. *J. Neurosci.* *27*, 12255–12266.
- Luskin, M.B. (1993). Restricted proliferation and migration of postnatally generated neurons derived from the forebrain subventricular zone. *Neuron* *11*, 173–189.
- Magdaleno, S., Jensen, P., Brumwell, C.L., et al. (2006). BGEM: an in situ hybridization database of gene expression in the embryonic and adult mouse nervous system. *PLoS Biol.* *4*, e86.
- Martin, C., and Zhang, Y. (2005). The diverse functions of histone lysine methylation. *Nat. Rev. Mol. Cell Biol.* *6*, 838–849.
- Ming, G.L., and Song, H. (2011). Adult neurogenesis in the mammalian brain: significant answers and significant questions. *Neuron* *70*, 687–702.
- Mishra, B.P., Zaffuto, K.M., Artinger, E.L., et al. (2014). The histone methyltransferase activity of MLL1 is dispensable for hematopoiesis and leukemogenesis. *Cell Rep.* *7*, 1239–1247.
- Mody, M., Cao, Y., Cui, Z., et al. (2001). Genome-wide gene expression profiles of the developing mouse hippocampus. *Proc. Natl Acad. Sci. USA* *98*, 8862–8867.
- Molofsky, A.V., He, S., Bydon, M., et al. (2005). Bmi-1 promotes neural stem cell self-renewal and neural development but not mouse growth and survival by repressing the p16Ink4a and p19Arf senescence pathways. *Genes Dev.* *19*, 1432–1437.
- Molofsky, A.V., Pardal, R., Iwashita, T., et al. (2003). Bmi-1 dependence distinguishes neural stem cell self-renewal from progenitor proliferation. *Nature* *425*, 962–967.
- Park, D.H., Hong, S.J., Salinas, R.D., et al. (2014). Activation of neuronal gene expression by the JMJD3 demethylase is required for postnatal and adult brain neurogenesis. *Cell Rep.* *8*, 1290–1299.
- Pastrana, E., Silva-Vargas, V., and Doetsch, F. (2011). Eyes wide open: a critical review of sphere-formation as an assay for stem cells. *Cell Stem Cell* *8*, 486–498.
- Qiu, J., Takagi, Y., Harada, J., et al. (2009). p27Kip1 constrains proliferation of neural progenitor cells in adult brain under homeostatic and ischemic conditions. *Stem Cells* *27*, 920–927.
- Schlett, K., and Madarasz, E. (1997). Retinoic acid induced neural differentiation in a neuroectodermal cell line immortalized by p53 deficiency. *J. Neurosci. Res.* *47*, 405–415.
- Schneider, R., Bannister, A.J., Myers, F.A., et al. (2004). Histone H3 lysine 4 methylation patterns in higher eukaryotic genes. *Nat. Cell Biol.* *6*, 73–77.
- Scholzen, T., and Gerdes, J. (2000). The Ki-67 protein: from the known and the unknown. *J. Cell. Physiol.* *182*, 311–322.
- Shilatifard, A. (2012). The COMPASS family of histone H3K4 methylases: mechanisms of regulation in development and disease pathogenesis. *Annu. Rev. Biochem.* *81*, 65–95.
- Subramanian, A., Tamayo, P., Mootha, V.K., et al. (2005). Gene set enrichment analysis: a knowledge-based approach for interpreting genome-wide expression profiles. *Proc. Natl Acad. Sci. USA* *102*, 15545–15550.
- Sun, Y., Nadal-Vicens, M., Misono, S., et al. (2001). Neurogenin promotes neurogenesis and inhibits glial differentiation by independent mechanisms. *Cell* *104*, 365–376.
- Tang, Z., Chen, W.Y., Shimada, M., et al. (2013). SET1 and p300 act synergistically, through coupled histone modifications, in transcriptional activation by p53. *Cell* *154*, 297–310.
- Telley, L., Govindan, S., Prados, J., et al. (2016). Sequential transcriptional waves direct the differentiation of newborn neurons in the mouse neocortex. *Science* *351*, 1443–1446.
- Tremblay, V., Zhang, P., Chaturvedi, C.P., et al. (2014). Molecular basis for DPY-30 association to COMPASS-like and NURF complexes. *Structure* *22*, 1821–1830.
- Tronche, F., Kellendonk, C., Kretz, O., et al. (1999). Disruption of the glucocorticoid receptor gene in the nervous system results in reduced anxiety. *Nat. Genet.* *23*, 99–103.
- Vallianatos, C.N., and Iwase, S. (2015). Disrupted intricacy of histone H3K4 methylation in neurodevelopmental disorders. *Epigenomics* *7*, 503–519.
- Villarreal-Campos, D., Gastaldi, L., Conde, C., et al. (2014). Rab-mediated trafficking role in neurite formation. *J. Neurochem.* *129*, 240–248.
- Yang, Z., Augustin, J., Chang, C., et al. (2014). The DPY30 subunit in SET1/MLL complexes regulates the proliferation and differentiation of hematopoietic progenitor cells. *Blood* *124*, 2025–2033.
- Yang, Z., Augustin, J., Hu, J., et al. (2015). Physical interactions and functional coordination between the core subunits of Set1/MLL complexes and the reprogramming factors. *PLoS One* *10*, e0145336.
- Yang, Z., Shah, K., Khodadadi-Jamayran, A., et al. (2016). Dpy30 is critical for maintaining the identity and function of adult hematopoietic stem cells. *J. Exp. Med.* *213*, 2349–2364.
- Yao, B., Christian, K.M., He, C., et al. (2016). Epigenetic mechanisms in neurogenesis. *Nat. Rev. Neurosci.* *17*, 537–549.
- Zhuo, L., Theis, M., Alvarez-Maya, I., et al. (2001). hGFAP-cre transgenic mice for manipulation of glial and neuronal function in vivo. *Genesis* *31*, 85–94.